

Preparation of Magnetic-Fluorescent Bifunctional Microrods as a Drug Delivery System via One-Step Electrospaying [†]

Junwei Xu ^{1,2}, Ping Li ^{1,2,*} and Yubo Fan ^{2,3,*}

¹ Key Laboratory for Biomechanics and Mechanobiology of Ministry of Education, School of Biological Science and Medical Engineering, Beihang University, Beijing 100191, China; 958102048@qq.com

² Beijing Advanced Innovation Centre for Biomedical Engineering, Beihang University, Beijing, 100191, China

³ School of Medical Science and Engineering, Beihang University, Beijing 100191, China

* Correspondence: liping@buaa.edu.cn (P.L.); yubofan@buaa.edu.cn (Y.F.); Tel.: +86-010-82339428

[†] Presented at the 1st International Electronic Conference on Pharmaceutics, 1–15 December 2020; Available online: <https://iecp2020.sciforum.net/>.

Received: date; Accepted: date; Published: date

Abstract: Magnetic-fluorescent bifunctional drug delivery system which possesses magnetic targeting and fluorescent tracing capabilities, effectively improves the delivery efficiency of drugs. With the in-depth study of the properties of non-spherical microparticles, it is found that the shape of the microparticles also plays a key role in drug delivery. Because of the unique shape, rod-like microparticles have exhibited great drug molecule metabolic dynamics and excellent anti-tumor effects during the process of treatment. In this study, Fe₃O₄/NaYF₄:Eu³⁺/PLGA magnetic-fluorescent bifunctional microrods were prepared via one-step electrospaying. Unlike other methods that require complicated steps or expensive equipment, one-step electrospaying is a facile and low-energy method. The prepared magnetic-fluorescent bifunctional microrods possessed uniform rod-like morphology. Compared with magnetic-fluorescent bifunctional microspheres in same volume, it was found that the microrods showed a lower water contact angle. The results of hysteresis curve and fluorescence spectrum suggested the excellent magnetic and fluorescent properties of magnetic-fluorescent bifunctional microrods. After co-cultured with A549 cells or endothelial cells, the cell viability testing results confirmed the wonderful biocompatibility of microrods. When the drug doxorubicin was loaded by the immersion method, the microrods showed a higher drug entrapment efficiency and drug-loading capacity in comparison with microspheres. In addition, microrods loaded with the same drug in weight showed stronger cytostatic effects after two days of co-culture with A549 cells. In summary, the magnetic-fluorescent bifunctional microrods prepared via one-step electrospaying will be promising candidates for biomedical applications in drug delivery, targeting and tracking.

Keywords: one-step electrospaying; magnetic-fluorescent bifunctional; microrods; drug delivery system; A549 cells

1. Introduction

In order to improve the efficiency of drug utilization, drug delivery system (DDS) was proposed and used for delivering and then releasing the drugs to the lesion as well as reducing the toxicity of drugs [1,2]. With the development of DDS, researchers paid more attention to the delivery targeting efficiency of DDS, especially that with magnetic targeting [3,4]. By wrapping the magnetic material in the DDS, the magnetic DDS would be guided to the diseased tissues or organs and realize the

targeted release of the drug under the action of an external magnetic field [5]. However, the magnetic DDS was poor in real-time tracking and observation and cannot be detected during the delivery process. Therefore, the method of combining fluorescent materials with magnetic targeting technology in DDS came into being, and the magnetic-fluorescent composite DDS received widespread attention [6–8]. With magnetic targeting and fluorescent labeling functions, the DDS could realize the integration of diagnosis and treatment such as biological imaging and drug delivery [9,10]. Cui et al. [11] designed a chitosan microcapsule, encapsulating oleic acid-modified Fe_3O_4 magnetic nanoparticles (MNPs) and green fluorescent dye coumarin 6, for targeted drug delivery and release. Li et al. [12] prepared a magnetic fluorescent bifunctional drug delivery system $\text{Fe}_3\text{O}_4/\text{TbBenzimidazole}(\text{Aspirin})_2/\text{Chitosan}$, which exhibited desirable fluorescent and magnetic properties.

For DDS, in addition to using magnetic or fluorescent materials to enhance targeting efficiency, the regulation in the morphology, size, and surface composition of the carrier also affects the therapeutic effect of the DDS [13]. For example, using liposomes as the carrier can help the DDS better reach to the lesions [14]. The strategy of preparing rod-shaped and urchin-like particles was also proposed to promote the cell phagocytosis efficiency by increasing the contact of DDS with cells [15]. Yi et al. [16] reported a self-sacrificing route for fabrication of the Ce/Tb co-doped GdPO hollow spheres under hydrothermal conditions, which showed excellent drug loading and release capabilities. Gratton et al. [17] indicated that the rate of Hella cells phagocytosed rod-like particles was four times than that of spherical particles of the same volume. However, compared with common spherical particles, the preparation of non-spherical particles is usually more difficult [15]. Previously, we prepared microrods by one-step electrospray. During the process of exploring DDS, it was found that rod-shaped DDS showed better drug molecular dynamics performance and better anti-tumor effects [18,19]. With the large specific surface area, high drug-loading capacity, long circulation time and high cell uptake efficiency, the rod-shaped DDS has a better effect than the spherical DDS in the treatment of cancer and other diseases [17,20,21].

In this study, we prepared magnetic-fluorescent bifunctional $\text{Fe}_3\text{O}_4/\text{NaYF}_4:\text{Eu}^{3+}/\text{PLGA}$ microrods via one-step electrospray. Embedding with Fe_3O_4 MNPs and fluorescent material $\text{NaYF}_4:\text{Eu}^{3+}$ nanoparticles (NPs), the obtained microrods showed a great rod shape in morphology. We studied the composition, magnetic and fluorescent properties, hydrophilic and hydrophobic properties and cytotoxicity of $\text{Fe}_3\text{O}_4/\text{NaYF}_4:\text{Eu}^{3+}/\text{PLGA}$ microrods in detail. Subsequently, doxorubicin (DOX) was loaded in the $\text{Fe}_3\text{O}_4/\text{NaYF}_4:\text{Eu}^{3+}/\text{PLGA}$ microrods and microspheres and the entrapment efficiency (EE) and drug-loading capacity (LC) of the two kinds of microparticles were calculated. For further compare the drug loading capacity, the cancer cells killing efficiency of drug-loading $\text{Fe}_3\text{O}_4/\text{NaYF}_4:\text{Eu}^{3+}/\text{PLGA}$ microrods and microspheres were explored with A549 lung cancer cells. The result suggested that the prepared magnetic-fluorescent bifunctional $\text{Fe}_3\text{O}_4/\text{NaYF}_4:\text{Eu}^{3+}/\text{PLGA}$ microrods were expected to be better used as the drug delivery carriers in the targeted therapy of tumors and other diseases.

2. Experiments

2.1. Materials

Poly (lactide-co-glycolide) (PLGA, $M_w = 2 \times 10^4$, LA:GA = 50:50) was bought from Jinan Daigang Biotechnology Co. Ltd. (Jinan, China). Tetrahydrofuran (THF) was provided by Shanghai Macklin Biochemical Technology Co. Ltd. (Shanghai, China). $\text{FeCl}_3 \cdot 6\text{H}_2\text{O}$ ($\geq 99.0\%$) and $\text{FeCl}_2 \cdot 4\text{H}_2\text{O}$ ($\geq 98.0\%$) were bought from Xilong Chemical Co. Ltd. (China). Diethylene glycol (DEG) was provided by Tianjin kwangfu Fine Chemicals Institute (Tianjin, China). $\text{Eu}(\text{NO}_3)_3 \cdot 6\text{H}_2\text{O}$ (99.99%), Hexafluoroisopropanol (HFIP) and doxorubicin (DOX) were bought from Aladdin Industrial Corporation (China). $\text{Y}(\text{NO}_3)_3 \cdot 6\text{H}_2\text{O}$ (99.0%), polyethyleneimine (PEI) and NaBF_4 were purchased from Shandong Xiya Chemical Industry Co. Ltd. (China). Absolute ethyl alcohol was bought from Beijing Tongguang Fine Chemical Company (Beijing, China). All reagents involved in this work were of analytical grade and directly used as-received without further purification.

2.2. Preparation of Fe₃O₄/NaYF₄: Eu³⁺/PLGA Microrods

Fe₃O₄ MNPs was prepared according to the method of Lotfi et al. [22] Briefly, 2.91 g FeCl₃·6H₂O and 1.07 g FeCl₂·4H₂O were dissolved in 100 mL deionized water and stirred at 800 rpm/min at 80 °C. Moreover, 20 mL of 25% ammonium hydroxide was injected into the solution after 15 min and then the mixture was stirred for 3 h. Finally, the black precipitate was washed four times with deionized water and ethanol and dried in a freeze drier at -50 °C for 24 h.

NaYF₄:Eu³⁺ NPs was produced by using the hydrothermal method [23,24]. Briefly, under vigorous stirring, 0.69 g Y(NO₃)₃·6H₂O, 0.09 g Eu(NO₃)₃·6H₂O and 0.17 g NaCl were mixed in 10 mL deionized water, 30 mL DEG and 10 mL 10 wt.% PEI solution were added into the mixture. Then, 0.2 g NaBF₄ solved in 5 mL deionized water was added and the mixture was stirred for 1 h. After transferred into a Teflon autoclave at 180 °C for 6 h, the product was washed four times with deionized water and ethanol and dried at 60 °C for 24 h.

Subsequently, for preparing Fe₃O₄/NaYF₄:Eu³⁺/PLGA microrods, as Figure 1 showed, 150 mg PLGA, 50 mg Fe₃O₄ MNPs and 50 mg NaYF₄:Eu³⁺ NPs were mixed in THF as the precursor solution. As for preparing Fe₃O₄/NaYF₄:Eu³⁺/PLGA microspheres, HFIP was used. During electrospinning, the precursor solution was loaded into a syringe, and placed on a pump. The collector was placed at 15 cm away from the needle, the voltage was set at 6–8 kV and the flow rate of the precursor solutions was 0.6 mL/h.

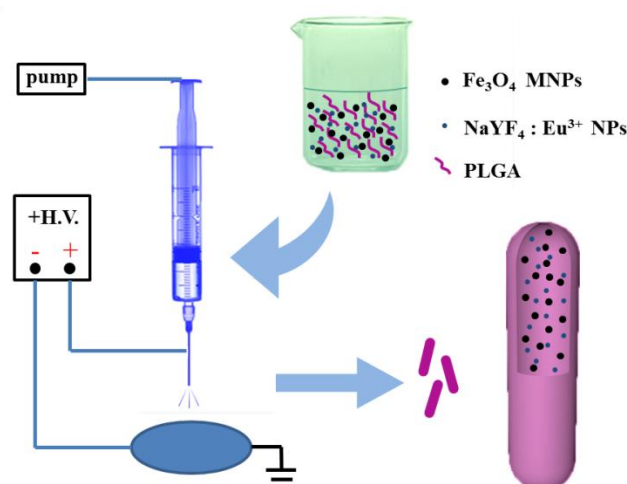


Figure 1. Schematic illustration of the preparation of the Fe₃O₄/NaYF₄:Eu³⁺/PLGA magnetic-fluorescent bifunctional microrods.

2.3. Drug Loading of Fe₃O₄/NaYF₄: Eu³⁺/PLGA Microrods

For loading drug, 30 mg prepared microrods or microspheres in was added into 3 mL DOX/deionized water solution (1 mg/mL) for 12 h. DOX-loaded Fe₃O₄/NaYF₄:Eu³⁺/PLGA microrods or microspheres was got after filtering and freeze-drying for 36 h. And EE and LC were calculated by using the followed formula, respectively.

$$EE (\%) = \frac{\text{Total DOX} - \text{Free DOX}}{\text{Total DOX}} \times 100\%$$

$$LC (\%) = \frac{\text{The weight of DOX}}{\text{The weight of DOX loaded microrods or microspheres}} \times 100\%$$

2.4. Characterization

Scanning electron microscopy (Quanta™ 250 FEG SEM, FEI, USA) was used to observe the morphology of Fe₃O₄/NaYF₄:Eu³⁺/PLGA microrods. In the SEM images, the lengths and diameters of atleast 200 microrods were measured by using the software Image J. The composition of the

microrods was tested by FTIR spectrometry (FTIR-1650, Tianjin Gang Dong Technology Development Co. Ltd., Tianjin, China) and Simultaneous Thermal Analyzer (STA, ZCT-A, Beijing Jingyi Gaoke Instrument Co. Ltd., Beijing, China). The Hydrophobicity-hydrophilicity was tested by using a contact measurement (JC2000FM, Powereach, Shanghai, China). Vibrating sample magnetometer (VSM, Laker Shore 7307, USA) and fluorescence spectrophotometer (FS5, Edinburgh, UK) were used to measure the magnetic and fluorescent properties, respectively. The OD values of DOX were detected by UV/VIS/NIR spectrophotometer (GENESYS 180, Thermo, Waltham, MA, USA) to evaluate the content of DOX.

2.5. Cell Experiments

2.5.1. Cell Culture

A549 cells were provided by Institute of Basic Medical Sciences of Chinese Academy of Medical Sciences. Human umbilical vein endothelial cells (HUVECs) were isolated from human umbilical cord veins collected from Peking University People's Hospital (Beijing, China). Informed consent was provided according to the Declaration of Helsinki. HUVECs were extracted and identified from umbilical cord vein tissue by using the published method [25]. HUVECs or A549 cells were grown in RPMI-1640 culture medium (Beijing Solarbio Technology Co. Ltd., Beijing, China) with 1% penicillin/streptomycin and 10% Fetal bovine serum (Zhejiang Tianhang Biotechnology Co. LTD., Zhejiang, China).

2.5.2. Cell Viability Assay

HUVECs or A549 cells with a density of 2×10^3 cells per well were seeded 96-well plates and co-cultured with 1 mg/mL PLGA microrods or microspheres for 1, 3 or 5 days. In vitro cell viability was measured with Cell Counting Kit-8 (CCK-8, Dojindo Laboratories, Kumamoto, Japan) in accordance with the manufacturer's instructions. And at day 5, cell viability assay by acridine orange (AO) staining (Beijing Solarbio Technology Co. Ltd., China) was also performed. Briefly, 150 μ L phosphate buffer saline solution containing 1.5 μ L AO was added into each well for 5 min incubation at room temperature. And the cells were observed by a fluorescence microscope (IX71, Olympus Inc., Tokyo, Japan).

A549 cells with a density of 5×10^3 cells per well were seeded in 96-well plates and co-cultured with DOX-loaded $\text{Fe}_3\text{O}_4/\text{NaYF}_4:\text{Eu}^{3+}/\text{PLGA}$ microrods or microspheres at the concentration of 0.1, 0.2, 0.5, 1, 2 or 5 mg/mL for 48 h. And A549 cells were also co-cultured with 1 mg/mL DOX-loaded $\text{Fe}_3\text{O}_4/\text{NaYF}_4:\text{Eu}^{3+}/\text{PLGA}$ microrods or microspheres for 12, 24, 48 or 72 h. The cell viabilities were performed by using CCK8.

2.6. Statistical Analysis

The results are expressed as mean \pm standard deviation. The statistical significance of results between groups was carried out by one-way ANOVA at a confidence level of 95% with SPSS 19.0 software. Differences were considered to be statistically significant for values of * $p < 0.05$ and ** $p < 0.01$.

3. Results

3.1. Morphology

The SEM images of the $\text{Fe}_3\text{O}_4/\text{NaYF}_4:\text{Eu}^{3+}/\text{PLGA}$ microrods were shown in Figure 1a,b. The microrods were successfully prepared and possessed uniform rod shape. The surface of the microrods was a bit rough because of the presence of Fe_3O_4 MNPs and $\text{NaYF}_4:\text{Eu}^{3+}$ NPs. The length distribution and diameter distribution of $\text{Fe}_3\text{O}_4/\text{NaYF}_4:\text{Eu}^{3+}/\text{PLGA}$ microrods were shown in Figure 1c,d, respectively. The mean length was $12.81 \pm 2.94 \mu\text{m}$ while the mean diameter was $1.20 \pm 0.31 \mu\text{m}$.

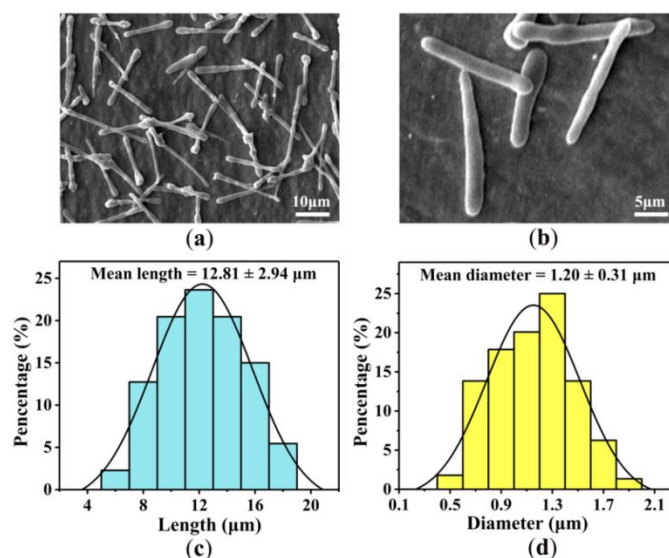


Figure 2. SEM images of $\text{Fe}_3\text{O}_4/\text{NaYF}_4:\text{Eu}^{3+}/\text{PLGA}$ microrods at different magnifications, (a) $\times 5000$, (b) $\times 10,000$; (c) length distribution and (d) diameter distribution of $\text{Fe}_3\text{O}_4/\text{NaYF}_4:\text{Eu}^{3+}/\text{PLGA}$ microrods.

3.2. Infrared Analysis and Thermal Stabilities

The FTIR spectra of PLGA and $\text{Fe}_3\text{O}_4/\text{NaYF}_4:\text{Eu}^{3+}/\text{PLGA}$ microrods were presented in Figure 3a. For the PLGA spectrum, the strong peak at 1754.9 cm^{-1} was assigned to the stretching vibration of C–O. The two absorption peaks at 1187.9 cm^{-1} and 1089.5 cm^{-1} represented the C–O–C stretching vibration of PLGA. The characteristic peaks of PLGA all appeared in the FTIR spectrum of $\text{Fe}_3\text{O}_4/\text{NaYF}_4:\text{Eu}^{3+}/\text{PLGA}$ microrods.

In Figure 3b, the TG curves of PLGA and $\text{Fe}_3\text{O}_4/\text{NaYF}_4:\text{Eu}^{3+}/\text{PLGA}$ microrods were similar and both of them experienced one loss stage of weight from 260 to 360 °C. Under 570 °C, the weight loss of PLGA reached 100%, while that of $\text{Fe}_3\text{O}_4/\text{NaYF}_4:\text{Eu}^{3+}/\text{PLGA}$ microrods was about 59%. It is because that the ratio of Fe_3O_4 MNPs and $\text{NaYF}_4:\text{Eu}^{3+}$ NPs to PLGA was 4:5 in the microrods, indicating that the samples had great thermal stability.

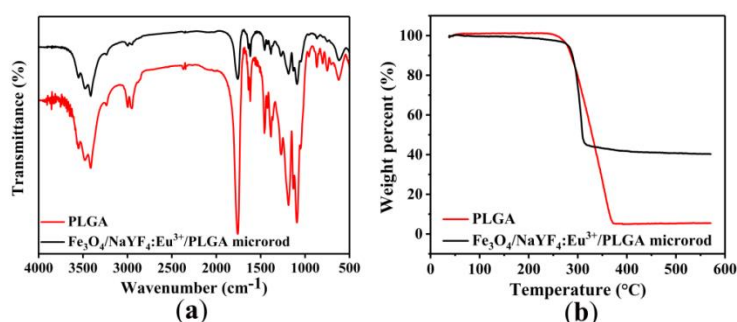


Figure 3. (a) FTIR spectra of PLGA and $\text{Fe}_3\text{O}_4/\text{NaYF}_4:\text{Eu}^{3+}/\text{PLGA}$ microrods; (b) TG curve of PLGA and $\text{Fe}_3\text{O}_4/\text{NaYF}_4:\text{Eu}^{3+}/\text{PLGA}$ microrods.

3.3. Magnetic and Fluorescent Properties

To study the magnetic property of the $\text{Fe}_3\text{O}_4/\text{NaYF}_4:\text{Eu}^{3+}/\text{PLGA}$ microrods, the hysteresis loops of the Fe_3O_4 MNPs and $\text{Fe}_3\text{O}_4/\text{NaYF}_4:\text{Eu}^{3+}/\text{PLGA}$ microrods under an applied field of 30 kOe were shown in Figure 4a,b. The saturation magnetization of the pure Fe_3O_4 MNPs was 67.4 emu/g. The Fe_3O_4 MNPs were embedded in the microrods, which could be observed under the optical microscope (Figure 4c), and the weight of Fe_3O_4 MNPs was only 2/9 of microrods, so the saturation magnetization of $\text{Fe}_3\text{O}_4/\text{NaYF}_4:\text{Eu}^{3+}/\text{PLGA}$ microrods was only 4.6 emu/g. Nevertheless, $\text{Fe}_3\text{O}_4/\text{NaYF}_4:\text{Eu}^{3+}/\text{PLGA}$ microrods still exhibited great magnetic properties.

The fluorescent property of $\text{Fe}_3\text{O}_4/\text{NaYF}_4:\text{Eu}^{3+}/\text{PLGA}$ microrods was studied at the excitation wavelength of 394 nm. The emission spectra of $\text{NaYF}_4:\text{Eu}^{3+}$ NPs and $\text{Fe}_3\text{O}_4/\text{NaYF}_4:\text{Eu}^{3+}/\text{PLGA}$ microrods were showed in Figure 4d,e, respectively. The broad peaks at about 593 and 615 nm corresponded to the transitions of $^5\text{D}_0 \rightarrow ^7\text{F}_1$ and $^5\text{D}_0 \rightarrow ^7\text{F}_2$ of Eu^{3+} , respectively. The intensity of emission spectra and the photograph in Figure 4f showed the red fluorescence suggested the excellent luminescent property of $\text{Fe}_3\text{O}_4/\text{NaYF}_4:\text{Eu}^{3+}/\text{PLGA}$ microrods which would be a good candidate for bioimaging and drug tracer.

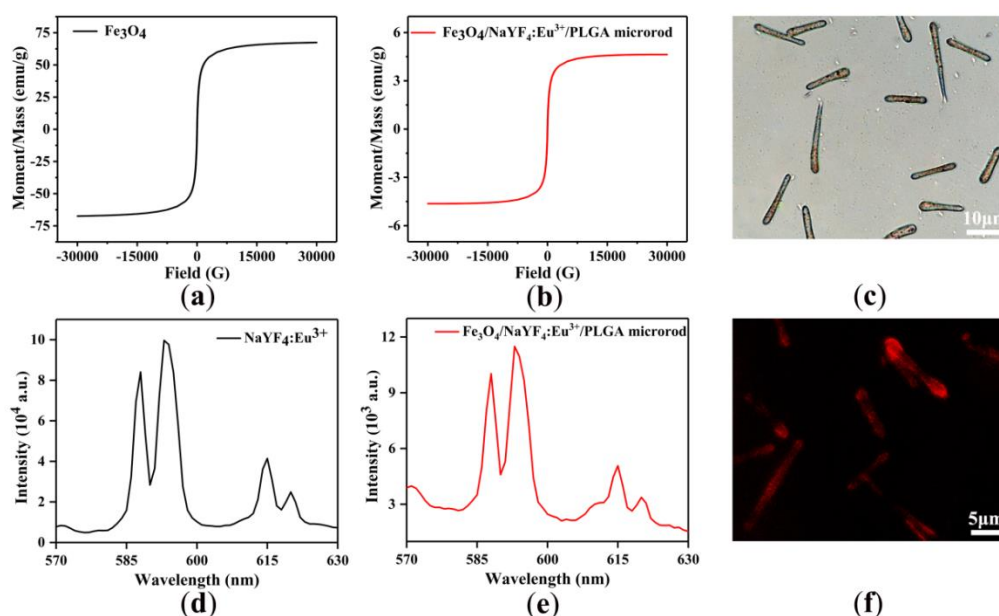


Figure 4. Hysteresis loop of (a) pure Fe_3O_4 MNPs and (b) $\text{Fe}_3\text{O}_4/\text{NaYF}_4:\text{Eu}^{3+}/\text{PLGA}$ microrods. (c) Optical microscope images of $\text{Fe}_3\text{O}_4/\text{NaYF}_4:\text{Eu}^{3+}/\text{PLGA}$ microrods. Emission spectra of (d) pure $\text{NaYF}_4:\text{Eu}^{3+}$ NPs and (e) $\text{Fe}_3\text{O}_4/\text{NaYF}_4:\text{Eu}^{3+}/\text{PLGA}$ microrods. (f) Fluorescent photograph of the $\text{Fe}_3\text{O}_4/\text{NaYF}_4:\text{Eu}^{3+}/\text{PLGA}$ microrods.

3.4. Hydrophobicity-Hydrophilicity

To examine the hydrophobicity–hydrophilicity of $\text{Fe}_3\text{O}_4/\text{NaYF}_4:\text{Eu}^{3+}/\text{PLGA}$ microrods, the contact angles of microrods and microspheres were measured. As shown in Figure 5a,b, the contact angles of $\text{Fe}_3\text{O}_4/\text{NaYF}_4:\text{Eu}^{3+}/\text{PLGA}$ microrods and microspheres were 113.3° and 123.0° , respectively. The microrods exhibited a smaller contact angle of approximately 9.7° than the microspheres, which suggested that microrods were more hydrophilic than microspheres.

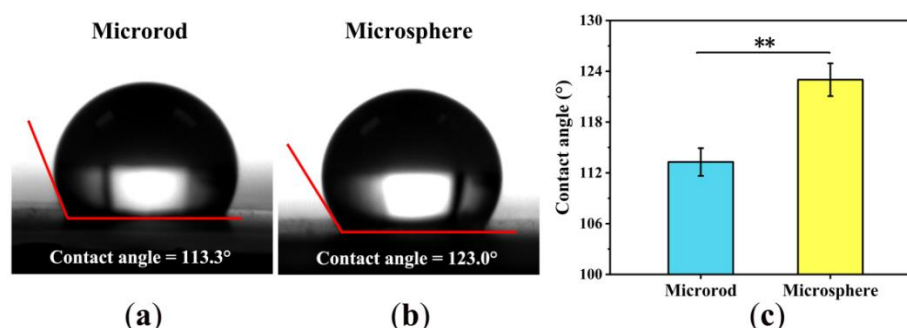


Figure 5. Images of water droplets on (a) $\text{Fe}_3\text{O}_4/\text{NaYF}_4:\text{Eu}^{3+}/\text{PLGA}$ microrods and (b) $\text{Fe}_3\text{O}_4/\text{NaYF}_4:\text{Eu}^{3+}/\text{PLGA}$ microspheres; (c) contact angles and of $\text{Fe}_3\text{O}_4/\text{NaYF}_4:\text{Eu}^{3+}/\text{PLGA}$ microrods and microspheres, $n = 3$.

3.5. Cytotoxicity

AO-stained fluorescence images showed that both normal cells (HUVECs) and tumor cells (A549 cells) were able to grow well in culture medium containing 1 mg/mL microrods or microspheres (Figure 6a). Cell viabilities in Figure 6b,c indicated that neither of microrods or microspheres showed significant cytotoxicity to HUVECs and A549 cells.

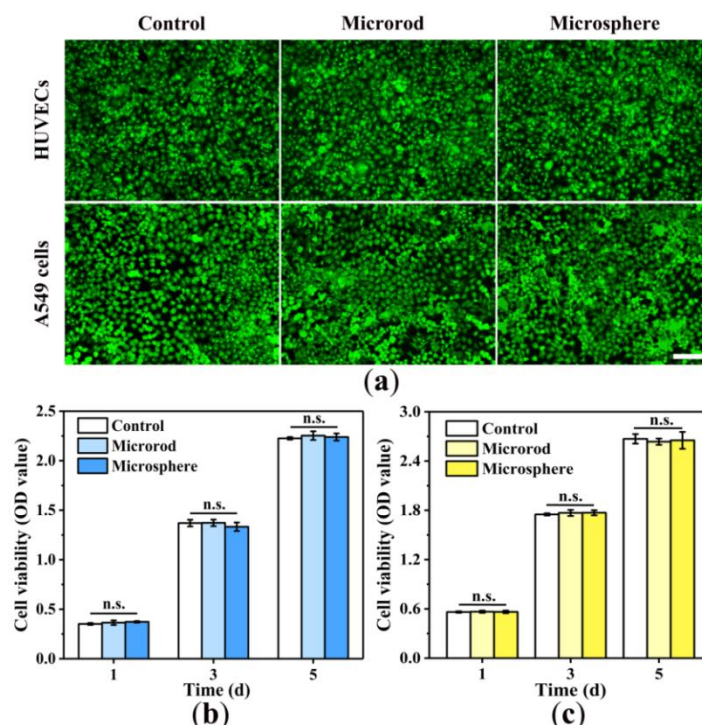


Figure 6. (a) Fluorescence images of HUVECs and A549 cells (stained with AO) cultured with microrods or microspheres at the concentration of 1 mg/mL for 5 d, scale bar: 100 μ m. In vitro cell relative viabilities of (b) HUVECs and (c) A549 cells co-cultured with $\text{Fe}_3\text{O}_4/\text{NaYF}_4:\text{Eu}^{3+}/\text{PLGA}$ microrods or microspheres at the concentration of 1 mg/mL for 1 d, 3 d and 5 d, $n = 3$.

3.6. Entrapment Efficiency and Drug-Loading Capacity

In order to compare the drug loading capacity of $\text{Fe}_3\text{O}_4/\text{NaYF}_4:\text{Eu}^{3+}/\text{PLGA}$ microrods and microspheres, the EE and LC of DOX loaded $\text{Fe}_3\text{O}_4/\text{NaYF}_4:\text{Eu}^{3+}/\text{PLGA}$ microrods and microspheres were calculated. As showed in Figure 7, the EE and LC of DOX loaded $\text{Fe}_3\text{O}_4/\text{NaYF}_4:\text{Eu}^{3+}/\text{PLGA}$ microrods were $9.153 \pm 0.506\%$ and $0.907 \pm 0.050\%$, higher than $8.368 \pm 0.259\%$ and $0.830 \pm 0.025\%$ of DOX loaded $\text{Fe}_3\text{O}_4/\text{NaYF}_4:\text{Eu}^{3+}/\text{PLGA}$ microspheres. The results suggested that the $\text{Fe}_3\text{O}_4/\text{NaYF}_4:\text{Eu}^{3+}/\text{PLGA}$ microrods possessed a better capacity for loading drugs than $\text{Fe}_3\text{O}_4/\text{NaYF}_4:\text{Eu}^{3+}/\text{PLGA}$ microspheres.

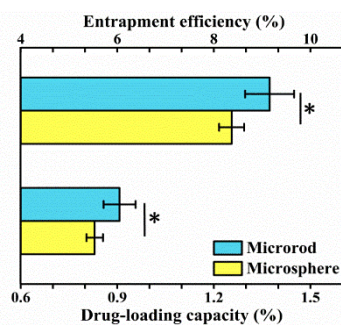


Figure 7. The calculated entrapment efficiency and drug-loading capacity of DOX loaded $\text{Fe}_3\text{O}_4/\text{NaYF}_4:\text{Eu}^{3+}/\text{PLGA}$ microrods and microspheres, $n = 3$.

3.7. Anti-Cancer Cell Efficiency

The anti-cancer cell efficiencies of DOX loaded $\text{Fe}_3\text{O}_4/\text{NaYF}_4:\text{Eu}^{3+}/\text{PLGA}$ microrods and microspheres were further evaluated. After co-cultured with DOX loaded $\text{Fe}_3\text{O}_4/\text{NaYF}_4:\text{Eu}^{3+}/\text{PLGA}$ microrods or microspheres at the concentrations from 0.1 to 5.0 mg/mL for 48 h, the viabilities of A549 cells were tested. As Figure 8a showed, the cell viabilities decreased with the concentration increment. At the concentrations from 0.1 to 1.0 mg/mL, the cell viabilities of A549 cells with DOX loaded $\text{Fe}_3\text{O}_4/\text{NaYF}_4:\text{Eu}^{3+}/\text{PLGA}$ microrods at 48 h were obviously lower than those of DOX loaded $\text{Fe}_3\text{O}_4/\text{NaYF}_4:\text{Eu}^{3+}/\text{PLGA}$ microspheres.

The viabilities of A549 cells co-cultured with 1.0 mg/mL DOX loaded $\text{Fe}_3\text{O}_4/\text{NaYF}_4:\text{Eu}^{3+}/\text{PLGA}$ microrods or microspheres for 12, 24, 48 and 72 h were tested. As Figure 8b showed, the cell viabilities decreased with the time went by. Both at 24 and 48 h, the cell viabilities of A549 cells with DOX loaded $\text{Fe}_3\text{O}_4/\text{NaYF}_4:\text{Eu}^{3+}/\text{PLGA}$ microrods were significantly lower than those of DOX loaded $\text{Fe}_3\text{O}_4/\text{NaYF}_4:\text{Eu}^{3+}/\text{PLGA}$ microspheres, which suggested the greater anti-cancer cell efficiency of DOX loaded $\text{Fe}_3\text{O}_4/\text{NaYF}_4:\text{Eu}^{3+}/\text{PLGA}$ microrods.

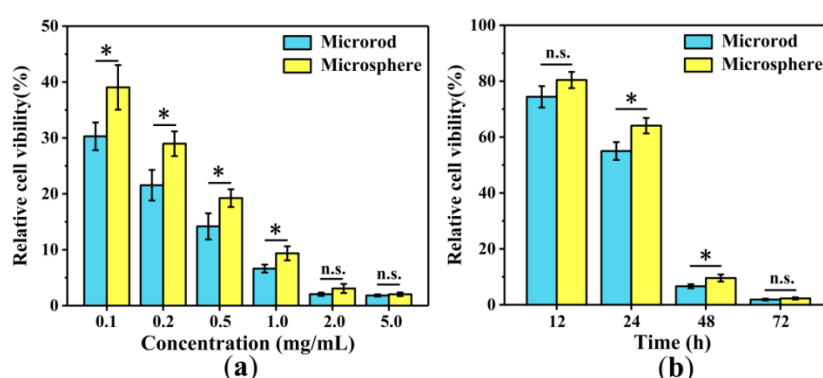


Figure 8. (a) In vitro A549 cell relative viabilities normalized to the untreated control after co-cultured with DOX loaded $\text{Fe}_3\text{O}_4/\text{NaYF}_4:\text{Eu}^{3+}/\text{PLGA}$ microrods or microspheres at different concentrations of 0.1, 0.2, 0.5, 1.0, 2.0 or 5.0 mg/mL for 48 h, $n = 3$. (b) In vitro A549 cell relative viabilities normalized to the untreated control at the concentration of 1.0 mg/mL for 12, 24, 48 and 72 h, $n = 3$.

4. Discussion

In this study, we developed a magnetic-fluorescent bifunctional $\text{Fe}_3\text{O}_4/\text{NaYF}_4:\text{Eu}^{3+}/\text{PLGA}$ drug delivery carriers. Electrospray is a simple and facile method to prepare microparticles, but the microparticles obtained are usually spherical. The conditions for one-step preparation of microrods by electrospray were studied [13], which greatly simplified the preparation process compared with other methods such as stretching technology [26] and the method of cutting long fibers [27]. After embedding with fluorescent materials and MNPs, the prepared magnetic-fluorescent bifunctional microrods still showed a great rod shape in morphology. The microrods possessed magnetic and fluorescent properties, which could provide the drug delivery carrier with magnetic targeting and fluorescent tracing functions. Although the saturation magnetic intensity and fluorescence intensity of the microrods were much lower compared with pure MNPs and fluorescent materials, it was because the MNPs and fluorescent materials were wrapped in PLGA, and the mass proportion were low. In addition, although the presence of magnetic materials may have a quenching effect on fluorescent materials [28,29], the fluorescence image still shows good fluorescence performance. The prepared magnetic-fluorescent bifunctional microrods were sufficient to induce magnetic response and fluorescence response [30].

Interestingly, there was a significant difference in hydrophilicity between $\text{Fe}_3\text{O}_4/\text{NaYF}_4:\text{Eu}^{3+}/\text{PLGA}$ microrods and microspheres after 30 min of electrospray, which may be related to the morphology of the microparticles. The study by Li et al. [30] pointed out that the water contact angle of microspheres is larger than that of red blood cell-like particles. Zhao et al. [31] fabricate surfaces with patterned multiscale roughness to render superhydrophobicity by

electrospraying technique. It might be due to the large number of microspheres spreading to form a shape similar to the hydrophobic array, so the water contact angle of the microspheres is larger. Generally speaking, proper hydrophilicity is conducive to enhancing cell affinity [32], indicating that rod-shaped particles should have better cell affinity than microspheres. In this study, PLGA, a kind of polymer with excellent biocompatibility, was used to as the material of carriers, and we also discussed the cytotoxicity of microrods and microspheres. The results showed that the microrods and microspheres had no obvious cytotoxicity to lung cancer cells and normal cells (HUVECs). This resulted indicated that the designed drug delivery carriers meet the basic requirements for drug delivery in vivo.

In order to ensure the same conditions as possible in the comparison between $\text{Fe}_3\text{O}_4/\text{NaYF}_4:\text{Eu}^{3+}/\text{PLGA}$ microrods and microspheres, physical immersion was used to prepare DOX-containing DDS. The results showed that the $\text{Fe}_3\text{O}_4/\text{NaYF}_4:\text{Eu}^{3+}/\text{PLGA}$ microrods exhibited higher encapsulation efficiency and drug loading capacity, which might due to the larger specific surface area in comparasion with microspheres. Meanwhile, at the same concentration, the microrods showed a faster cell killing effects. On the one hand, this may be related to the relatively large amount of drug loaded. On the other hand, due to the higher specific surface area of the microrods, the release of the drug was relatively faster, which caused the faster cancer killing effect of DOX-loaded $\text{Fe}_3\text{O}_4/\text{NaYF}_4:\text{Eu}^{3+}/\text{PLGA}$ microrods.

5. Conclusions

Magnetic-fluorescent bifunctional $\text{Fe}_3\text{O}_4/\text{NaYF}_4:\text{Eu}^{3+}/\text{PLGA}$ microrods have been successfully prepared via one-step electrospray. The obtained $\text{Fe}_3\text{O}_4/\text{NaYF}_4:\text{Eu}^{3+}/\text{PLGA}$ microrods showed a good rod shape in morphology. The results from hysteresis loop suggested that the microrods had outstanding magnetic properties. Fluorescence emission spectra and fluorescence images indicated the excellent fluorescence performance of the microrod. Compared with microspheres, microrods have better hydrophilic property, but both AO staining and CCK8 results indicated that there was no obvious cytotoxicity of $\text{Fe}_3\text{O}_4/\text{NaYF}_4:\text{Eu}^{3+}/\text{PLGA}$ microrods and microspheres, whether for A549 lung cancer cells or normal endothelial cells (HUVECs). Moreover, drug-loading experiments suggested that the microrods had a higher entrapment efficiency and drug-loading capacity for the drug, which promotes the drug-loading $\text{Fe}_3\text{O}_4/\text{NaYF}_4:\text{Eu}^{3+}/\text{PLGA}$ microrods to have stronger killing effects to cancer cells. In short, this rod-shaped drug carrier, $\text{Fe}_3\text{O}_4/\text{NaYF}_4:\text{Eu}^{3+}/\text{PLGA}$ microrods, with magnetic-fluorescent bifunctional have a good prospect in the field of drug delivery.

Author Contributions: P.L. and Y.F. conceived and designed the experiments; J.X. performed the experiments; J.X. analyzed the data; P.L. and Y.F. contributed reagents/materials/analysis tools; J.X. wrote the paper. All authors have read and agreed to the published version of the manuscript.

Funding: This study was supported by funds from National Natural Science Foundation of China (NSFC) Research Grants (61871014, 52071008, 11827803, 11421202), and it was also supported by Beijing Natural Science Foundation (7191006).

Conflicts of Interest: The authors declare no conflict of interest.

Abbreviations

The following abbreviations are used in this manuscript:

PLGA	Poly (lactide-co-glycolide)
THF	Tetrahydrofuran
DEG	Diethylene glycol
HFIP	Hexafluoroisopropanol
DOX	doxorubicin
PEI	polyethyleneimine
DDS	drug delivery system
MNP	magnetic nanoparticle
NP	nanoparticle

EE	entrapment efficiency
LC	drug-loading capacity
HUVEC	human umbilical vein endothelial cell
CCK-8	Cell Counting Kit-8
AO	Acridine Orange
PBS	phosphate buffer saline

References

1. Qian, C.M. Drug delivery systems (DDS): I .The definition, characteristic and classification of DDS. *Northwest Pharm. J.* **1995**, *10*, 133–136.
2. Davoodi, P.; Lee, L.Y.; Xu, Q.; Sunil, V.; Sun, Y.; Soh, S.; Wang, C.-H. Drug delivery systems for programmed and on-demand release. *Adv. Drug Deliv. Rev.* **2018**, *132*, 104–138.
3. Grifantini, R.; Taranta, M.; Gherardini, L.; Naldi, I.; Parri, M.; Grandi, A.; Giannetti, A.; Tombelli, S.; Lucarini, G.; Ricotti, L.; et al. Magnetically driven drug delivery systems improving targeted immunotherapy for colon-rectal cancer. *J. Control Release* **2018**, *280*, 76–86.
4. Liu, Y.L.; Chen, D.; Shang, P.; Yin, D.C. A review of magnet systems for targeted drug delivery. *J. Control Release* **2019**, *302*, 90–104.
5. Asfour, A.; Raouf, K.; Yonnet, J.P. Software Defined Radio (SDR) and Direct Digital Synthesizer (DDS) for NMR/MRI instruments at low-field. *Sensors* **2013**, *13*, 16245–16262.
6. Han, L.; Ma, Q.; Dong, X. Direct electrospinning construction of nanocables with electrical conductive-magnetic core and insulative-photoluminescent sheath. *RSC Adv.* **2015**, *5*, 95674–95681.
7. Lu, X.; Zhang, Z.; Xia, Q.; Hou, M.; Yan, C.; Chen, Z.; Xu, Y.; Liu, R. Glucose functionalized carbon quantum dot containing organic radical for optical/MR dual-modality bioimaging. *Mater. Sci. Eng. C Mater. Biol. Appl.* **2018**, *82*, 190–196.
8. Feng, X.; Wang, X.; Zhang, D.; Feng, F.; Yao, L.; Ma, G. One-step Preparation of Monodisperse Multifunctional Macroporous Particles through a Spontaneous Physical Process. *Small* **2018**, *14*, 1703570.
9. Marcelo, G.A.; Lodeiro, C.; Capelo, J.L.; Lorenzo, J.; Oliveira, E. Magnetic, fluorescent and hybrid nanoparticles: From synthesis to application in biosystems. *Mater. Sci. Eng. C Mater. Biol. Appl.* **2020**, *106*, 110104.
10. Mandal, K.; Jana, D.; Ghorai, B.K.; Jana, N.R. AIEgen-Conjugated Magnetic Nanoparticles as Magnetic-Fluorescent Bioimaging Probes. *ACS Appl. Nano Mater.* **2019**, *2*, 3292–3299.
11. Cui, X.; Guan, X.; Zhong, S.; Chen, J.; Zhu, H.; Li, Z.; Xu, F.; Chen, P.; Wang, H. Multi-stimuli responsive smart chitosan-based microcapsules for targeted drug delivery and triggered drug release. *Ultrason. Sonochem.* **2017**, *38*, 145–153.
12. Li, P.; Qi, B.; Li, K.; Xu, J.; Song, Y.; Kang, D.; Fan, Y. Development of Magnetic-Fluorescent Bifunctional Drug Delivery System with Dual Drug Content and Enhanced Fluorescence. *J. Nanosci. Nanotechnol.* **2018**, *18*, 8094–8098.
13. Li, P.; Xu, J.; Qi, B.; Li, K.; Gu, X.; Niu, X.; Fan, Y. One-Step Preparation of Poly(Lactide-Co-Glycolide) Fiber Rods Embedding with Luminescent Materials as a Drug Delivery System via Electrospray. *Nanosci. Nanotechnol. Lett.* **2018**, *10*, 1287–1291.
14. Huang, W.; Zhang, J.; Dorn, H.C.; Zhang, C. Assembly of Bio-Nanoparticles for Double Controlled Drug Release. *PLoS ONE* **2013**, *8*, e74679.
15. Yu, B.; Cong, H.; Peng, Q.; Gu, C.; Tang, Q.; Xu, X.; Tian, C.; Zhai, F. Current status and future developments in preparation and application of nonspherical polymer particles. *Adv. Colloid Interface Sci.* **2018**, *256*, 126–151.
16. Yi, Z.; Lu, W.; Qian, C.; Zeng, T.; Yin, L.; Wang, H.; Rao, L.; Liu, H.; Zeng, S. Urchin-like Ce/Tb co-doped GdPO₄ hollow spheres for in vivo luminescence/X-ray bioimaging and drug delivery. *Biomater. Sci.* **2014**, *2*, 1404–1411.
17. Gratton, S.E.; Ropp, P.A.; Pohlhaus, P.D.; Luft, J.C.; Madden, V.J.; Napier, M.E.; DeSimone, J.M. The effect of particle design on cellular internalization pathways. *Proc. Natl. Acad. Sci. USA* **2008**, *105*, 11613–11618.
18. Zhang, H.; Liu, Y.; Chen, M.; Luo, X.; Li, X. Shape effects of electrospun fiber rods on the tissue distribution and antitumor efficacy. *J. Control Release* **2016**, *244*, 52–62.

19. Wei, Y.; Li, X.; Zhu, X.; et al. Injectable Electrospun Composite Short Nanofibers Incorporated with Doxorubicin for Cancer Therapy. In *Abstract for the 2017 International Forum on Biomedical Textile Materials, 17–19 May 2017*; 2017.
20. Chauhan, V.P.; Popovic, Z.; Chen, O.; Cui, J.; Fukumura, D.; Bawendi, M.G.; Jain, R.K. Fluorescent nanorods and nanospheres for real-time in vivo probing of nanoparticle shape-dependent tumor penetration. *Angew. Chem. Int. Ed. Engl.* **2011**, *50*, 11417–11420.
21. Richards, D.M.; Endres, R.G. Target shape dependence in a simple model of receptor-mediated endocytosis and phagocytosis. *Proc. Natl. Acad. Sci. USA* **2016**, *113*, 6113–6118.
22. Lotfi, S.; Bahari, A.; Mahjoub, S. In vitro biological evaluations of Fe₃O₄ compared with core–shell structures of chitosan-coated Fe₃O₄ and polyacrylic acid-coated Fe₃O₄ nanoparticles. *Res. Chem. Intermed.* **2019**, *45*, 3497–3512.
23. Zhang, W.k.; Huang, H.; Tao, X.Y. Enhanced luminescence properties of hexagonal-phase NaYF₄: Eu³⁺/microrods by annealing treatment. *Adv. Mater. Res.* **2011**, 335–336, 1009–1013.
24. Liang, X.; Hu, Y.; Ma, X.; Wang, Y.; Fan, J.; Hu, X. A novel template-free and one-step method to fabricate hollow mesoporous structured upconversion luminescent NaYF₄: Yb³⁺, Er³⁺ nanoparticles. *Mater. Lett.* **2014**, *129*, 107–110.
25. Kang, H.; Fan, Y.; Sun, A.; Deng, X. Compositional or charge density modification of the endothelial glycocalyx accelerates flow-dependent concentration polarization of low-density lipoproteins. *Exp. Biol. Med.* **2011**, *236*, 800–807.
26. Champion, J.A.; Katare, Y.K.; Mitragotri, S. Making polymeric micro- and nanoparticles of complex shapes. *Proc. Natl. Acad. Sci. USA* **2007**, *104*, 11901–11904.
27. Omidinia-Anarkoli, A.; Boesveld, S.; Tuvshindorj, U.; Rose, J.C.; Haraszti, T.; De Laporte, L. An Injectable Hybrid Hydrogel with Oriented Short Fibers Induces Unidirectional Growth of Functional Nerve Cells. *Small* **2017**, *13*, doi:10.1002/smll.201702207.
28. Li, P.; Li, K.; Niu, X.; Fan, Y. Electrospaying magnetic-fluorescent bifunctional Janus PLGA microspheres with dual rare earth ions fluorescent-labeling drugs. *RSC Adv.* **2016**, *6*, 99034–99043.
29. Peng, H.; He, Y.; Tian, X.; Wen, J.; Zhang, L. LSPR effects in a magnetic–luminescent heterostructure for efficient enhanced luminescence performance. *New J. Chem.* **2019**, *43*, 304–311.
30. Li, P.; Qi, B.; Li, K.; Xu, J.; Liu, M.; Gu, X.; Niu, X.; Fan, Y. Study on the formation and properties of red blood cell-like Fe₃O₄/TbLa₃(Bim)₁₂/PLGA composite particles. *RSC Adv.* **2018**, *8*, 12503–12516.
31. Al-Milaji, K.N.; Zhao, H. Fabrication of superoleophobic surfaces by mask-assisted electrospay. *Appl. Surf. Sci.* **2017**, *396*, 955–964.
32. Li, Q.; Wang, Z.; Zhang, S.; Zheng, W.; Zhao, Q.; Zhang, J.; Wang, L.; Wang, S.; Kong, D. Functionalization of the surface of electrospun poly(epsilon-caprolactone) mats using zwitterionic poly(carboxybetaine methacrylate) and cell-specific peptide for endothelial progenitor cells capture. *Mater. Sci. Eng. C Mater. Biol. Appl.* **2013**, *33*, 1646–1653.

Publisher’s Note: MDPI stays neutral with regard to jurisdictional claims in published maps and institutional affiliations.



© 2020 by the authors. Submitted for possible open access publication under the terms and conditions of the Creative Commons Attribution (CC BY) license (<http://creativecommons.org/licenses/by/4.0/>).